ACS OMEGA

Open Access

http://pubs.acs.org/journal/acsodf

Article

Study of the Fe_3O_4@ZIF-8@Sor Composite Modified by Tannic Acid for the Treatment of Sorafenib-Resistant Hepatocellular Carcinoma

Jianqiao Kong, Song Xu, Yang Dai, Yi Wang, Yun Zhao,* and Peng Zhang*

Cite This: *ACS Omega* 2023, 8, 39174−39185

Read Online

ACCESS | Metrics & More | Article Recommendations

ABSTRACT: Chemotherapeutic agents fail in clinical chemotherapy in the absence of targeting and acquired resistance. We, therefore, synthesized Fe_3O_4@ZIF-8@Sor@TA nanocomposite drugs based on the drug delivery properties of nanomaterials. ZIF-8 is a nanomaterial with a porous structure that can load anticancer drugs. The nanodrug used the paramagnetic property of Fe_3O_4 to deliver sorafenib (Sor) precisely to the tumor site, then used the pH responsiveness of ZIF-8 to slowly release Sor in the tumor microenvironment, and finally used tannic acid (TA) to inhibit P-glycoprotein to suppress the Sor resistance. The results of material characterization presented that the prepared material was structurally stable and was able to achieve a cumulative drug release of 38.2% at pH 5.0 for 72 h. The good biocompatibility of the composite was demonstrated by in vitro and in vivo experiments, which could improve antitumor activity and reduce Sor resistance through magnetic targeting TA. In conclusion, the Fe_3O_4@ZIF-8@Sor@TA material prepared in this study demonstrated high antitumor activity in hepatocellular carcinoma treatment, promising to reduce drug resistance and providing a novel research approach for cancer treatment.

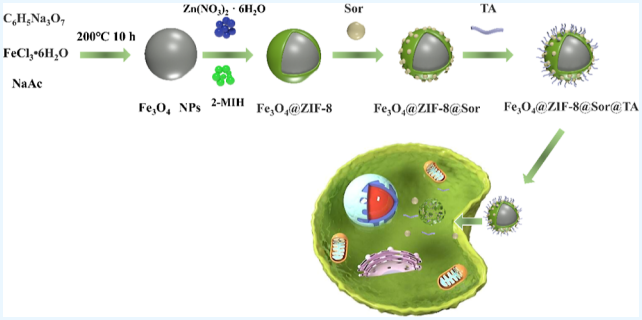

1. INTRODUCTION

Hepatocellular carcinoma (HCC) is one of the most common malignancies, ranking fifth in incidence worldwide.[1] It is mainly treated with surgery and chemotherapy, which are the main treatment strategies for this disease.[2,3] Due to the concealment of HCC, most patients are identified at an advanced stage with poor surgical outcomes.[4] Additionally, chemotherapy has its limitations since its long-term application may result in the development of drug resistance in cancer cells.[5]

Many researchers have adopted nanomaterials as drug carriers in recent years to improve therapeutic efficacy for HCC. Lin et al.[6] prepared resveratrol-modified mesoporous silica nanoparticles (Res-MSNs) with a more pronounced therapeutic effect on gastric cancer and improved biocompatibility with normal tissues when compared to Res alone. Nanomaterials, as previously described, can serve as effective carriers of chemotherapeutic agents and have promising applications in improving therapeutic effects, enhancing bioavailability, and reducing side effects. There are varying nanomaterials, such as graphene oxide,[7] hydroxyapatite,[8] nanopolymers,[9] and liposomes.[10] Different nanomaterials may confer new properties while loading drugs. Xu et al.[11] prepared a MoS_2 nanosheet, which has both drug-loading and photothermal capabilities. Based on these findings, this study generated a tumor treatment method combining nanomaterials and chemotherapeutic agents.

Metal−organic frameworks (MOFs) are novel materials with porous structures[12] that are applicated in the delivery of biomolecular drugs.[13] There are various types of MOFs, among which zeolitic imidazolate framework-8 (ZIF-8) is a typical MOF material with the advantages of mild synthesis conditions[14] and adjustable particle size and pore size.[15] Yu et al.[16] took advantage of the drug-loading capacity of ZIF-8 to load the anticancer drug curcumin (Cur) and encapsulated hyaluronic acid (HA). Their experimental results confirmed that the composites have good drug-loading capacity and slow release in a physiological environment but strong drug release capacity under acidic conditions, indicating good biosafety and a high tumor inhibition rate of the composites. Although ZIF-8 has tumor site stability and pH acid responsiveness,[17] its nanomedicine targeting ability needs to be improved. Specific active targeting and externally driven targeting are the two main approaches for tumor-specific targeted therapies,[18] and the former can rely on specific targets on the surface of nanocarriers for active targeting.[19] Using differences in

Received: June 21, 2023
Accepted: August 30, 2023
Published: September 12, 2023

https://doi.org/10.1021/acsomega.3c04215
ACS Omega 2023, 8, 39174−39185

Scheme 1. Flowchart for the Preparation of Fe_3O_4@ZIF-8@Sor@TA

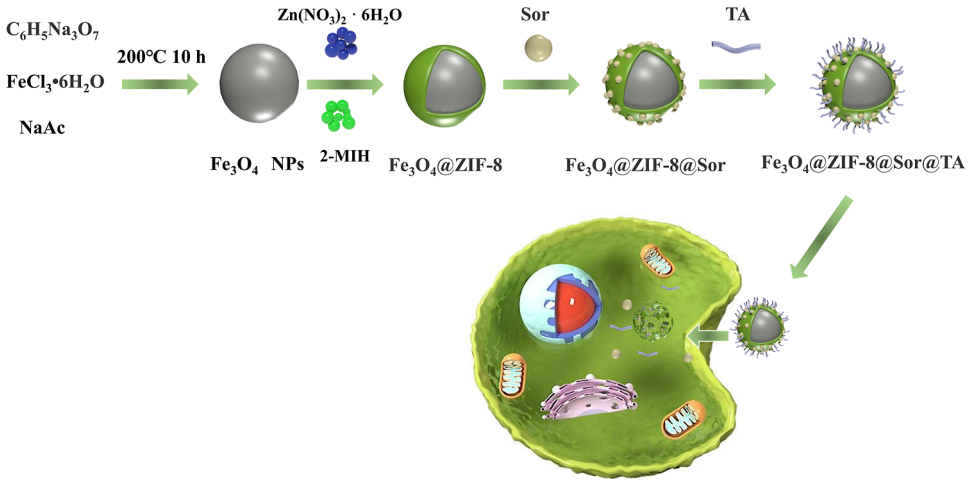

electrical charge or magnetic forces, externally driven targeting can be used to target tumors.[20] Fe_3O_4 is a superparamagnetic nanoparticle[21] with applications in tumor therapy and diagnosis,[22] magnetothermal therapy,[23] and drug delivery.[24] Moreover, Fe_3O_4 exhibits low toxicity and has a long circulation time in the body, which can improve the circulation time of chemotherapeutics.[25] Based on these previous investigations, this study used Fe_3O_4 to improve ZIF-8 targeting and enhance chemotherapeutic drug-loading and delivery for cancer treatment.

Sorafenib (Sor) is a multikinase inhibitor that represses tumor proliferation by reducing it and is a common first-line chemotherapeutic agent in clinical practice.[26,27] However, HCC patients who take Sor may experience adverse events such as gastrointestinal reactions, skin disorders, and hypertension,[27] thus affecting the effectiveness of chemotherapy. Tannic acid (TA) is a kind of natural polyphenol rich in catechols and pyrogallic acids, widely found in nature.[28] It has anticancer activity,[29] antiviral activity,[30] and anti-multidrug resistance.[31] For instance, TA treatment could inhibit PI3K/AKT, a well-known cancer-promoting signal, thereby decreasing the cancer's proliferative ability.[32] In addition, Naus et al.[33] explored the therapeutic effects of TA synergic chemotherapy, demonstrating that TA can affect the efficacy of chemotherapeutics by influencing drug efflux mechanisms. Considering the multiple cancer-suppressing effects, several nanodrugs for cancer therapy were designed based on TA.[34]

Based on this knowledge, a novel composite nanodrug was designed by loading Fe_3O_4@ZIF-8 with the chemotherapeutic agent Sor and modifying it with TA, which is capable of reducing drug resistance, improving anticancer ability as well as targeting, and reducing drug resistance. The preparation processes are depicted in Scheme 1. The composite had a large specific surface area and good pH responsiveness, a high drug-loading rate, and a significant release effect in the tumor microenvironment. Furthermore, Fe_3O_4 provided magnetic targeting to the composite, which was able to enhance the accumulation of anticancer drugs at tumor sites under magnetic conditions. Meanwhile, encapsulating TA on the surface of Fe_3O_4@ZIF-8@Sor prevented the early leakage of Sor and reduced drug resistance. This synthesized nanodrug could effectively suppress HCC cells, achieve tumor targeting, and hamper tumor cell growth to realize the purpose of safe and effective therapy.

2. METHODS

2.1. Reagents and Instruments. All chemicals used in this study were analytical pure reagents. Iron(III) chloride hexahydrate ($FeCl_3 \cdot 6H_2O$, AR, 99%), ethylene glycol ($(CH_2OH)_2$, AR, 98%), sodium acetate (NaAc, AR, 99%), trisodium citrate dihydrate ($C_6H_5Na_3O_7$, 98%), poly(styrene sulfonate)sodium salt (PSS), methanol (AR, 99.5%), zinc nitrate hexahydrate ($Zn(NO_3)_2 \cdot 6H_2O$, AR, 99%), 2-methylimidazole (98%), ethanol, Sor (99%), and TA (95%) were all purchased from Shanghai Aladdin Biochemical Technology Co., Ltd. (China)

2.2. Preparation of Materials. *2.2.1. Preparation of Fe_3O_4 Nanoparticles.* 1.14 g of $FeCl_3 \cdot 6H_2O$ was added to 50 mL of $(CH_2OH)_2$, dissolved ultrasonically, and stirred on a magnetic stirrer for 30 min before adding 2.4 g of NaAc and 0.65 g of $C_6H_5Na_3O_7$, and stirring for another 30 min. Afterward, the mixed solution was transferred to a 100 mL reactor and placed at 200 °C for 10 h. Following the reaction, the solution was cooled to room temperature before being rinsed several times with ethanol until the supernatant was clear by centrifugation and finally placed into an oven at 60 °C for 12 h to dry.

2.2.2. Preparation of Fe_3O_4@ZIF-8. 30 mg of Fe_3O_4 nanoparticles was added to 30 mL of an aqueous solution containing 0.3% PSS. They were sonicated for 20 min for dissolution before being recovered with a magnet and washed three times with deionized water. Next, samples were resuspended in 30 mL of methanol solution containing 0.225 g of $Zn(NO_3)_2 \cdot 6H_2O$ and 0.622 g of 2-methylimidazole and sonicated for 5 min to homogenize the solution. After the solution was mechanically stirred at room temperature for 1 h, samples were washed several times with ethanol and then dried in an oven at 70 °C for 12 h.

2.2.3. Preparation of Fe_3O_4@ZIF-8@Sor. 30 mg of Fe_3O_4 nanoparticles was added to 30 mL of an aqueous solution containing 0.3% PSS. They were sonicated for 20 min for dissolution, and the samples were recovered with a magnet and washed three times with deionized water. Next, samples were resuspended in 30 mL of methanol solution containing 0.225 g of $Zn(NO_3)_2 \cdot 6H_2O$, 0.622 g of 2-methylimidazole, and 0.01 g of Sor and sonicated for 5 min to homogenize the solution. After the solution was mechanically stirred at room temperature for 1 h, samples were washed several times with ethanol and finally placed in a freezing machine for freeze-drying.

https://doi.org/10.1021/acsomega.3c04215
ACS Omega 2023, 8, 39174−39185

2.2.4. Preparation of Fe_3O_4@ZIF-8@Sor@TA. 30 mg of Fe_3O_4 nanoparticles was added to 30 mL of an aqueous solution containing 0.3% PSS. They were sonicated for 20 min for dissolution, and the samples were recovered with a magnet and washed three times with deionized water. Next, samples were resuspended in 30 mL of methanol solution containing 0.225 g of $Zn(NO_3)_2{\cdot}6H_2O$, 0.622 g of 2-methylimidazole, and 0.01 g of Sor and sonicated for 5 min to homogenize the solution. After being mechanically stirred at room temperature for 1 h, the solution was added with 10 mg of TA, followed by 4 h of stirring. Finally, samples were washed several times with ethanol, placed in a freeze dryer, and then set aside.

2.3. Material Characterization. The morphology and dimensions of materials were characterized using a JEM-2100 electron microscope (JEOL Ltd., Japan) and a transmission electron microscope (TEM). The various groups of the materials were characterized using a Nicolet iS50 FTIR spectrometer (Thermo Fisher Scientific). The crystalline structures of samples were characterized using an X-ray diffractometer (ARL XTRA, Switzerland, 2θ = 5−80°). The magnetization properties of the materials were tested using the 7400 Series VSM (Lake Shore Cryotronics, USA). The drug and material drug loadings were tested using a UV-visible spectrophotometer (UV−vis, UV-2450, Shimadzu, Japan). The potential of the material was characterized using a zeta potential analyzer (NanoBrook Omni, USA).

2.4. Drug Release In Vitro. The release of Sor from Fe_3O_4@ZIF-8@Sor@TA was measured by dialysis. 10 mg of Fe_3O_4@ZIF-8@Sor@TA was dispersed into 3 mL of PBS solution, and then the solution was transferred into a dialysis bag (MWCO = 3.5 kDa). The dialysis bags were immersed in 30 mL of PBS with pH values of 5.0 and 7.5, and 2 mL of PBS dialysis exudate solution was withdrawn at different time points while an equal amount of fresh PBS solution was added to the solution. UV absorbance tests were performed on the extracted solutions to investigate the relationship between Sor release and time.

$$\text{Sor loading} = \text{total Sor input} - \text{free Sor} \quad (1)$$

where 'free Sor' refers to the amount of free Sor washed off each time after loading the drug.

$$\text{encapsulating ratio \%} = \frac{\text{Sor loading}}{\text{total Sor input}} \times 100 \quad (2)$$

$$\text{loading ratio \%} = \frac{\text{Sor loading}}{(\text{Sor loading} + \text{carrier mass})} \times 100 \quad (3)$$

2.5. Cell Culture. Human HCC cell lines (HepG2: BNCC338070 and BEL-7402: BNCC359871) were purchased from BeNa Culture Collection (China). A human HCC HepG2/Sor-resistant cell line (BFN6072012699) was purchased from Qingqi (Shanghai) Biology (China). The human hepatic cell line (LX-2) was purchased from Abiowell (China). HepG2, HepG2/Sor-resistant, and LX-2 cell lines were seeded into a high glucose-DMEM (Hyclone) medium containing 10% fetal bovine serum (FBS; Gibco) and 1% double antibody (Hyclone). BEL-7402 cells were plated into RPMI-1640 (Gibco) medium containing 10% FBS and 1% double antibody (Hyclone). All cell lines were cultured at 37 °C in a 5% CO_2 incubator.

2.5.1. Cytotoxicity Testing of Materials. The CCK-8 method was utilized to detect the cytotoxicity of each material to different cells. HepG2, BEL-7402, and LX-2 cells in the logarithmic phase were plated in 96-well plates (1×10^4 cells/well), respectively, and maintained in the incubator for 24 h. After the cells grew to about 80%, Fe_3O_4 (50 μg/mL), Fe_3O_4@ZIF-8 (50 μg/mL), TA (10 μg/mL), and Sor, Fe_3O_4@ZIF-8@Sor, Fe_3O_4@ZIF-8@Sor@TA, and Fe_3O_4@ZIF-8@Sor@TA (magnetic) with Sor concentration at 10 μg/mL were added to 96-well plates, respectively. All materials were set up in 5 replicate wells, and incubation was continued for 24 h with PBS as the control group. After incubation, the medium with the material was aspirated and replaced with an equal amount of medium containing 10% CCK-8. Incubation was continued in the incubator for 4 h. The 96-well plates were then removed, and their OD values at 450 nm were detected using an enzyme marker (PerkinElmer, USA) to calculate cell viability. The cytotoxicity of Fe_3O_4@ZIF-8@Sor@TA and Fe_3O_4@ZIF-8@Sor@TA (magnetic) with different Sor concentrations (1, 5, 10, 15, and 20 μg/mL) on HepG2 and BEL-7402 cells was tested using the CCK-8 method with PBS as the control group. The cell survival rates of Fe_3O_4@ZIF-8@Sor@TA-treated HepG2 and BEL-7402 were compared, and the HepG2 cells that were more sensitive to Fe_3O_4@ZIF-8@Sor@TA were selected to continue the experiments.

2.5.2. IC_{50} Assay of Nanomaterials on Sor Resistance. The CCK-8 method was utilized in this assay. HepG2/Sor-resistant cells (1×10^4 cells/well) were seeded in 96-well plates and cultured for 24 h. Free Sor, Fe_3O_4@ZIF-8@Sor, Fe_3O_4@ZIF-8@Sor@TA, and Fe_3O_4@ZIF-8@Sor@TA + magnetic-induced materials were added at concentrations of 0, 1, 5, 10, and 20 μg/mL, respectively, and the incubation was continued for 24 h. The inhibition rate of the material against HepG2/Sor was determined using the CCK-8 method after the incubation was completed, and the IC_{50} value was calculated to obtain the reversal fold of Sor according to the formula (RI = IC_{50} of Sor/IC_{50} of Fe_3O_4@ZIF-8@Sor@TA).

2.5.3. Living and Dead Cell Staining as Observed by Confocal Laser Scanning Microscopy. HepG2 and HepG2/Sor-resistant cells (1×10^4 cells/well) were seeded in 96-well plates and cultured overnight in an incubator. Cells were treated with PBS, Fe_3O_4@ZIF-8, Fe_3O_4@ZIF-8@Sor, Fe_3O_4@ZIF-8@Sor@TA, and Fe_3O_4@ZIF-8@Sor@TA (magnetic) (Sor concentration was 9 μg/mL), respectively, and incubated for 24 h. After washing with PBS three times, 10 μL of AM and 10 μL of propidium iodide (PI) were added for simultaneous staining of living and dead cells for 15 min. Photographs were taken using an inverted fluorescence microscope to observe the effect of magnetism on cell viability.

2.5.4. Cellular Uptake. Since Sor is an anticancer drug that does not fluoresce, in order to examine the cellular uptake of the composite, it was first necessary to construct a composite material with fluorescent labeling. Fe_3O_4@ZIF-8@C-6 and Fe_3O_4@ZIF-8@C-6@TA with fluorescence were prepared by replacing Sor with coumarin-6 (C-6). HepG2/Sor-resistant cells (5×10^5 cells/well) were plated in 6-well plates and cultured for 24 h. Free C-6, Fe_3O_4@ZIF-8@C-6, TA-pretreated Fe_3O_4@ZIF-8@C-6, and Fe_3O_4@ZIF-8@C-6@TA (the concentration of C-6 was 9 μg/mL) were added with PBS as the control group, and the incubation was continued for 4 h. Cells were then rinsed 3 times with PBS and fixed using 4% paraformaldehyde (stained for 15 min). 5 μL of rhodamine B-labeled phalloidin stains (5 μg/mL) was added to stain the cytoskeleton for 40 min, followed by DAPI staining for 15 min.

https://doi.org/10.1021/acsomega.3c04215
ACS Omega 2023, 8, 39174−39185

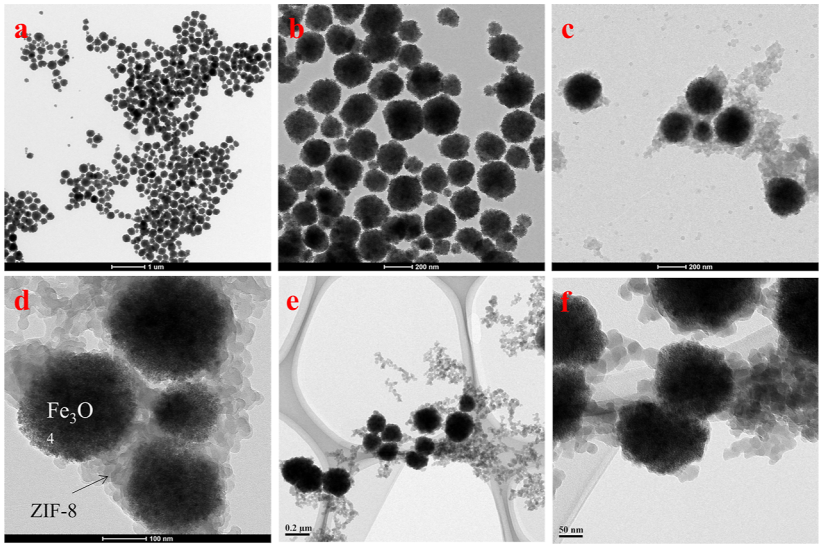

Figure 1. TEM images of each material. (a,b) TEM images of Fe_3O_4; (c,d) TEM images of Fe_3O_4@ZIF-8; and (e,f) TEM images of Fe_3O_4@ZIF-8@Sor@TA.

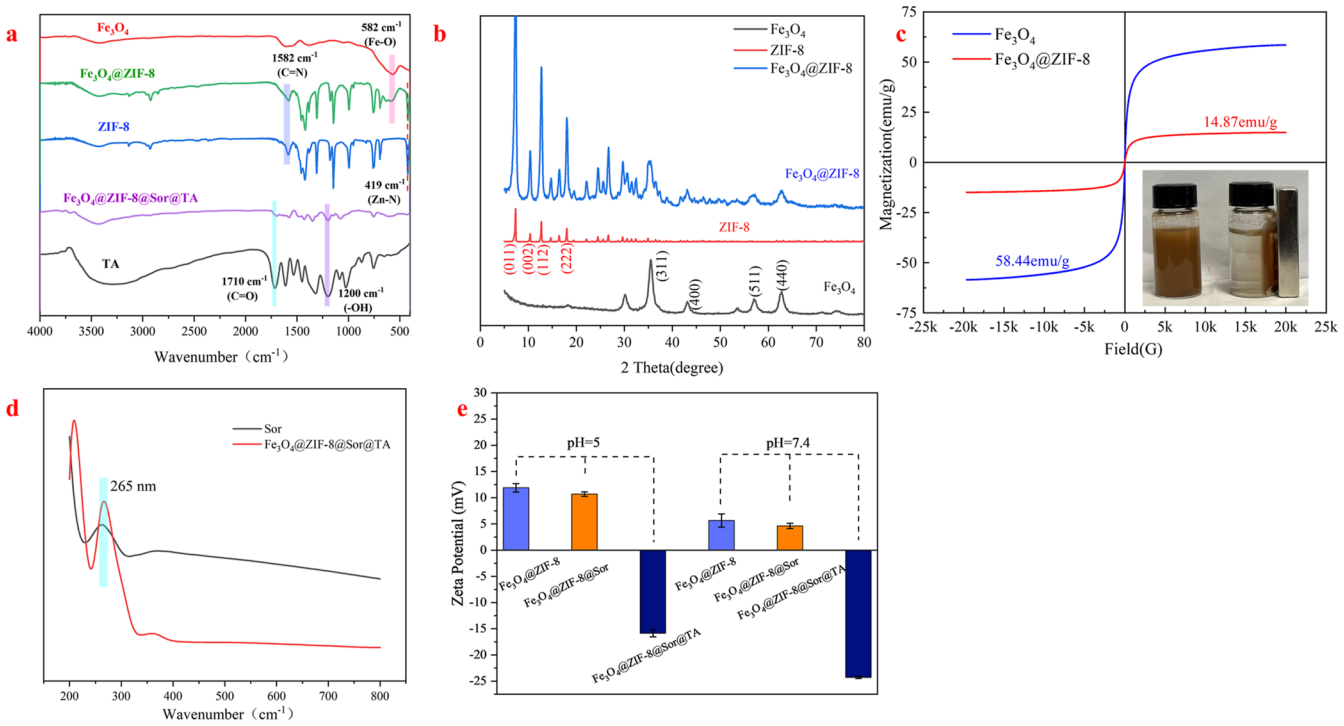

Figure 2. Characterization diagram of each material. (a) FTIR plots of TA, Fe_3O_4, ZIF-8, Fe_3O_4@ZIF-8, and Fe_3O_4@ZIF-8@Sor@TA; (b) XRD plots of Fe_3O_4, ZIF-8, and Fe_3O_4@ZIF-8; (c) magnetic hysteresis loop plots of Fe_3O_4 and Fe_3O_4@ZIF-8; (d) UV spectra of Sor and Fe_3O_4@ZIF-8@Sor@TA; and (e) zeta potential plots of Fe_3O_4@ZIF-8, Fe_3O_4@ZIF-8@Sor, and Fe_3O_4@ZIF-8@Sor@TA.

Finally, cellular uptake was observed using a CLSM (FluoView FV1000, Olympus).

2.5.5. Cell Apoptosis. HepG2 and HepG2/Sor-resistant cells (5×10^5 cells/well) were seeded in 6-well plates and incubated in an incubator for 24 h. The PBS-treated group was the control. After the cells grew to 80% confluence, free Sor, Fe_3O_4@ZIF-8@Sor, Fe_3O_4@ZIF-8@Sor@TA, and Fe_3O_4@ZIF-8@Sor@TA (magnetic) (the concentration of Sor was 9 μg/mL) were added to the cells, and incubation was continued for 24 h. After incubation, cells were harvested, washed, and resuspended. Cells with different treatments were stained using the Annexin V-FITC/PI double-staining kit (BestBio, China). The obtained samples were analyzed by flow cytometry (BD FACSVerse, USA) to evaluate the apoptosis in each group.

2.6. In Vivo Antitumor Study. The tumor-bearing mice used in this study were Balb/c nude mice (18−20 g) from Shanghai SLAC (China). 1 mL of HepG2/Sor cell suspension (1×10^6 cells/mL) was injected into the right axillary subcutis of nude mice to establish a mouse model for HCC.

2.6.1. In Vivo Antitumor Activity. To evaluate the in vivo antitumor ability of the composites, the established tumor-bearing mice were assigned into four groups ($n = 5$) and were injected with the same concentration and volume of PBS, free Sor, Fe_3O_4@ZIF-8@Sor@TA, and Fe_3O_4@ZIF-8@Sor@TA

https://doi.org/10.1021/acsomega.3c04215
ACS Omega 2023, 8, 39174−39185

(magnetic) (Sor concentration was 9 μg/mL, 0.05 mL) in the tail vein every 2 days for the whole treatment period of 21 days. During the treatment, the diameter of the mouse tumor was measured every 2 days, the volume of the tumor was calculated, and the weight of the mice was recorded. At the end of the treatment cycle, mice were euthanized, the tumors and organs (heart, living, spleen, kidneys, and lungs) were excised and removed, and the tumors were weighed and photographed. The excised organs and tumors were then fixed using 4% paraformaldehyde, paraffin-embedded, and histologically sectioned. Hematoxylin−eosin (H&E) staining was done to observe the histopathology of each tissue section under an optical microscope (Leica, Wetzlar, Germany).

2.6.2. In Vivo Near-Infrared Fluorescence Imaging. To examine the distribution of the composite in the organism, the lipid-soluble fluorescent dye DiR was chosen to replace Sor, and Fe_3O_4@ZIF-8@DiR@TA was prepared with the same preparation method. Mice were assigned into 4 groups (n = 5) and injected with DiR (0.5 mg/kg) and Fe_3O_4@ZIF-8@DiR@TA (magnetic) in the tail vein. The fluorescence intensity (excitation wavelength: 745 nm) was observed at 2, 4, 6, 8, 12, 24, and 48 h after drug injection using the IVIS spectrum in vivo imaging system. After 48 h of injection, mice were euthanized, and the tumor tissue and organs (heart, liver, spleen, lungs, and kidneys) were excised for ex vivo fluorescence imaging in the same procedures.

3. RESULTS

3.1. Nanomaterial Structure and Characterization. Fe_3O_4 nanoparticles were prepared by the solvothermal method, and Fe_3O_4@ZIF-8 was prepared by mechanical stirring of Fe_3O_4 nanoparticles with 2-methylimidazole and $Zn(NO_3)_2{\cdot}6H_2O$. TEM images of Fe_3O_4 nanoparticles are shown in Figure 1a,b. TEM images of Fe_3O_4@ZIF-8 material are depicted in Figure 1c,d. As plotted in Figure 1a,b, Fe_3O_4 nanoparticles were uniformly sized and dispersed, with a size of about 150 nm. Figure 1c,d illustrates that ZIF-8 was wrapped on the surface of the Fe_3O_4 core in the form of shells with uniform dispersion and that the wrapping of the ZIF-8 shell did not change the overall spherical appearance of Fe_3O_4,[35] indicating that ZIF-8 was successfully wrapped on the surface of Fe_3O_4 microspheres. TEM images of Fe_3O_4@ZIF-8@Sor@TA (Figure 1e,f) revealed that TEM images of Fe_3O_4@ZIF-8@Sor@TA and Fe_3O_4@ZIF-8 were similar in morphology, and the addition of Sor and modification of TA did not change the morphology of Fe_3O_4@ZIF-8 material.

The FTIR characterization was performed to discuss the situation of the groups on Fe_3O_4, Fe_3O_4@ZIF-8, and Fe_3O_4@ZIF-8@Sor@TA materials. The characterization results are presented in Figure 2a. For Fe_3O_4 nanoparticles, the peaks at 1385 and 1607 cm^{-1} were caused by carboxyl (−COOH) vibrations, while the characteristic peak of the stretching vibration of Fe_3O_4 particles (Fe−O) appeared at a wavelength of 582 cm^{-1}.[36] The peaks at the 500−1350 and 1350−1500 cm^{-1} ranges in the ZIF-8 spectrogram were caused by the planar bending and stretching of the imidazole ring. Meanwhile, the peaks at 2500−3500 cm^{-1} mainly originated from the stretching vibrations of groups such as −NH and −OH. The stretching vibrations at 1582 and 1667 cm^{-1} corresponded to −C═N and −NH, respectively, while the peak at 419 cm^{-1} was caused by the vibration of the Zn−N group.[37] In addition, the Fe_3O_4@ZIF-8 spectrogram was similar to the ZIF-8 spectrogram, with the only difference being that the characteristic peak of Fe_3O_4 (Fe−O) appears at 582 cm^{-1} in the Fe_3O_4@ZIF-8 spectrogram,[37] which proved that Fe_3O_4@ZIF-8 was synthesized successfully. FTIR characterization of TA and the final product Fe_3O_4@ZIF-8@Sor@TA was also performed after loading Sor and modifying TA. As revealed by IR maps of both materials, peaks at 1200 cm^{-1} mainly originated from the (−OH) bending vibrations on TA, whereas peaks appearing at 3000−3500 cm^{-1} were due to the TA (−OH) stretching vibrations.[38] The characteristic (C═O) peak of TA was also observed at 1710 cm^{-1}.[39] In summary, TA was successfully modified to a Fe_3O_4@ZIF-8 surface.

The crystalline structures of Fe_3O_4, ZIF-8, and Fe_3O_4@ZIF-8 were shown in the X-ray diffraction (XRD) patterns (Figure 2b). The characteristic peaks of Fe_3O_4 and ZIF-8 could be found in the XRD patterns of Fe_3O_4@ZIF-8, specifically, ZIF-8 and Fe_3O_4@ZIF-8 at 2θ = 7.4, 10.3, 12.9, and 18.0° for ZIF-8 corresponding to (011), (002), (112), and (222) crystal planes.[37,40] The peaks of Fe_3O_4@ZIF-8 at 35.1°(311), 43.2°(400), 56.7°(511), and 62.5°(440) were compatible with the standard card of Fe_3O_4, and there were no other spurious peaks on the XRD pattern of Fe_3O_4 with good crystal form. These results proved the successful synthesis of Fe_3O_4@ZIF-8.

The results of the magnetic hysteresis loop of samples measured by VSM are presented in Figure 2c. The magnetic saturation (MS) values of Fe_3O_4 and Fe_3O_4@ZIF-8 particles were 58.44 and 14.87 emu/g, respectively. High MS values implied that Fe_3O_4 had a strong magnetic response, in contrast, the MS values of Fe_3O_4@ZIF-8 were lower than those of Fe_3O_4, owing to the encapsulation of the ZIF-8 shell. Fe_3O_4@ZIF-8 particles were highly dispersed in aqueous solutions and can react quickly in an externally strong magnetic field.

To determine the Sor loading, UV spectrophotometric analysis was conducted on Sor and Fe_3O_4@ZIF-8@Sor@TA. As depicted in Figure 2d, the Sor UV spectrum had a maximum absorption peak at 265 nm.[38] Similarly, the Fe_3O_4@ZIF-8@Sor@TA UV spectrum also showed a maximum absorption peak around 265 nm, indicating that Sor had been successfully wrapped to Fe_3O_4@ZIF-8. The results of zeta potential tests on Fe_3O_4@ZIF-8, Fe_3O_4@ZIF-8@Sor, and Fe_3O_4@ZIF-8@Sor@TA are presented in Figure 2e. Zeta potentials of Fe_3O_4@ZIF-8, Fe_3O_4@ZIF-8@Sor, and Fe_3O_4@ZIF-8@Sor@TA at pH = 5 were 11.9, 10.7, and −15.87 mV, respectively. Zeta potentials of Fe_3O_4@ZIF-8, Fe_3O_4@ZIF-8@Sor, and Fe_3O_4@ZIF-8@Sor@TA at pH = 7.4 were 5.6, 4.63, and −24.3 mV, respectively. The positive charge originally carried by the material changed to a negative charge, indicating that TA was modified to the material.[41]

3.2. In Vitro Drug Release. We explored the drug release behavior of Fe_3O_4@ZIF-8@Sor@TA nanomaterials in a normal in vivo environment and a tumor microenvironment by changing the pH value of PBS. The amount of material prepared in this experiment was about 50 mg, and the final loading amount of Sor was about 4 mg. The encapsulating ratio was about 40%, and the loading ratio was about 7.4%. A 50 mL (1 mg/mL) solution of Fe_3O_4@ZIF-8@Sor@TA nanomaterials was prepared for drug release experiments. Figure 3 shows the Sor release rate of Fe_3O_4@ZIF-8@Sor@TA nanomaterial over time at pH = 5 and pH = 7.4. The release rate of Sor reached 38.2% at pH = 5 and h = 72 h, while at pH = 7.4 and h = 72 h, the release rate of Sor was only 9.54%. The main reason was that ZIF-8 in nanomaterials was pH-responsive, and under acidic conditions, ZIF-8 disintegrated

https://doi.org/10.1021/acsomega.3c04215
ACS Omega 2023, 8, 39174−39185

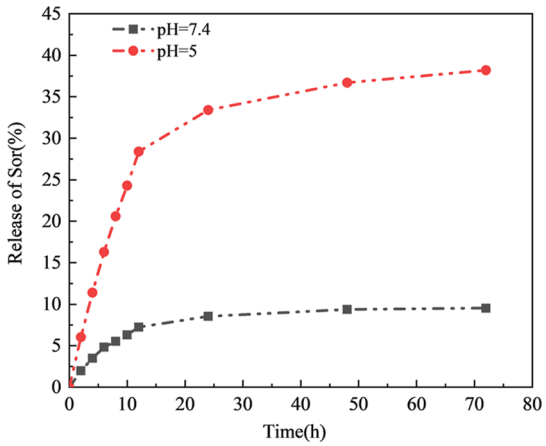

Figure 3. Plot of the Sor release rate of Fe_3O_4@ZIF-8@Sor@TA at different pH values (5 and 7.4).

and thus released the encapsulated Sor. While under weak alkaline conditions, ZIF-8 did not disintegrate, and the released Sor was limited. Hence, Sor could be fully released in the tumor microenvironment to achieve a tumor treatment effect.

3.3. Cytotoxicity of Nanocomposites. The toxic effect of nanodrugs on cells was an important indicator to evaluate their safety and efficacy. Figure 4a–c presents the cytotoxicity of different nanomaterials for different cells tested using the CCK-8 method. First, Figure 4a illustrates that the prepared Fe_3O_4, Fe_3O_4@ZIF-8, and TA were biocompatible, with cell survival rates of more than 90% in HepG2, BEL-7402, and LX-2 (50 μg/mL). When the same concentrations of Sor, Fe_3O_4@ZIF-8@Sor, Fe_3O_4@ZIF-8@Sor@TA, and Fe_3O_4@ZIF-8@Sor@TA (magnetic) were added to the above cells for 24 h of incubation, HepG2 and BEL-7402 cells were damaged to different degrees, and the cell survival rate was the highest for Sor and the lowest for Fe_3O_4@ZIF-8@Sor@TA (magnetic), indicating that Fe_3O_4@ZIF-8@Sor@TA had the strongest ability to kill tumors when magnetic targeting and chemotherapy acted synergistically. In contrast, the survival rate of LX-2 cells remained above 90%, indicating that the TA encapsulation somewhat improved their biocompatibility. Besides, its lower cytotoxicity to normal cells may also be caused by the fact that ZIF-8 responded to the tumor microenvironment and was stable when neutral or basic. To further investigate the suppressive effect of Fe_3O_4@ZIF-8@Sor@TA on HCC cells, we set up a series of concentration gradients to examine the killing effect of different concentrations of Fe_3O_4@ZIF-8@Sor@TA on HepG2 and BEL-7402 cells under magnetic and non-magnetic conditions. The results are depicted in Figure 4b,c. Cell survival rates of HepG2 and BEL-7402 were negatively correlated with the concentration of Fe_3O_4@ZIF-8@Sor@TA, with a higher concentration indicating a lower cell survival rate. The affinity of Fe_3O_4@ZIF-8@Sor@TA for HepG2 cells was higher than that of BEL-7402 cells. When the Sor concentration in materials was 15 μg/mL, the survival rates of Fe_3O_4@ZIF-8@Sor@TA and Fe_3O_4@ZIF-8@Sor@TA (magnetic) in HepG2 cells were about 19 and 16%, respectively. The change in cell survival rate became insignificant when the material concentration continued to increase.

3.4. Effect of Materials on Sor Resistance in HCC. Since Fe_3O_4@ZIF-8@Sor@TA showed the highest killing effect on HepG2 cells, HepG2 cells were selected for the following experiment. During HCC chemotherapy, the acquired drug resistance was one of the main reasons for poor efficacy, tumor recurrence, and treatment failure. The

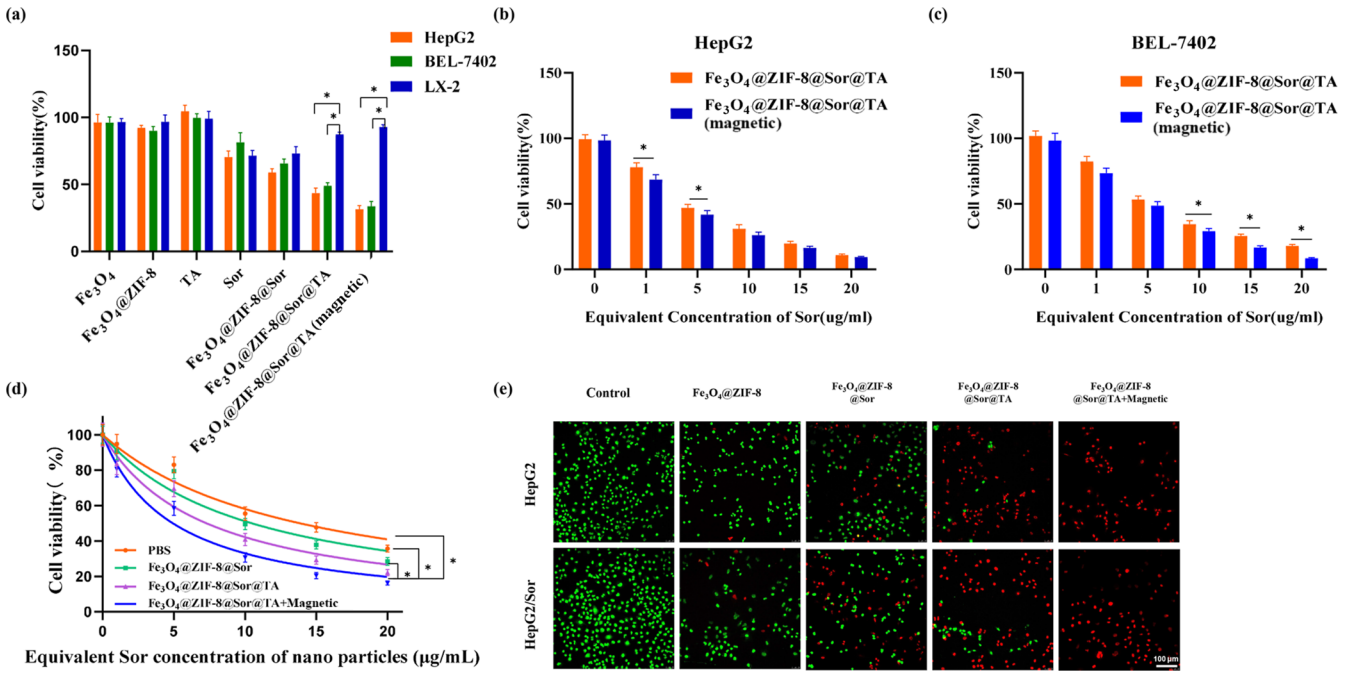

Figure 4. Cytotoxicity and cell survival tests of different materials on different cells. (a) Effect of Fe_3O_4, Fe_3O_4@ZIF-8, TA, Sor, Fe_3O_4@ZIF-8@Sor, Fe_3O_4@ZIF-8@Sor@TA, and Fe_3O_4@ZIF-8@Sor@TA (magnetic) on cell survival of HepG2, BEL-7402, and LX-2; (b) effect of Fe_3O_4@ZIF-8@Sor@TA and Fe_3O_4@ZIF-8@Sor@TA (magnetic) on HepG2 cell survival; (c) Fe_3O_4@ZIF-8@Sor@TA and Fe_3O_4@ZIF-8@Sor@TA (magnetic) on BEL-7402 cell viability; (d) Fe_3O_4@ZIF-8@Sor, Fe_3O_4@ZIF-8@Sor@TA, and Fe_3O_4@ZIF-8@Sor@TA (magnetic) on HepG2/Sor cell survival; and (e) fluorescence images of calcein AM (green)/PI (red) co-stained cells.

https://doi.org/10.1021/acsomega.3c04215
ACS Omega 2023, 8, 39174−39185

modification of TA in the Fe_3O_4@ZIF-8@Sor@TA synthesized in this experiment had the opportunity to reverse the drug resistance phenomenon. Figure 4d presents that when different materials were added to HepG2/Sor cells, they were damaged to some extent. The cell survival rate was the lowest in the Fe_3O_4@ZIF-8@Sor@TA (magnetic) group. After calculation, the IC_{50} values of Sor, Fe_3O_4@ZIF-8@Sor, Fe_3O_4@ZIF-8@Sor@TA, and Fe_3O_4@ZIF-8@Sor@TA (magnetic) were about 14, 10, 7, and 5, respectively. The reversal folds of Fe_3O_4@ZIF-8@Sor@TA and Fe_3O_4@ZIF-8@Sor@TA (magnetic) were close to 2 and 3 times, respectively, indicating that the prepared Fe_3O_4@ZIF-8@Sor@TA could reduce Sor resistance and could treat HepG2/Sor-resistant cells well under the induction of magnetism.

3.5. Killing Ability of Nanomaterials as Observed by Fluorescence Imaging. To observe the effect of materials on cell viability more clearly, living and dead cells were stained using AM and PI and imaged using inverted fluorescence microscopy. As plotted in Figure 4e, when Fe_3O_4@ZIF-8 was co-cultured with HepG2 or HepG2/Sor cells, almost no red fluorescence (dead cells) was observed, indicating that Fe_3O_4@ZIF-8 itself did not affect cell viability. When Fe_3O_4@ZIF-8@Sor was added, the green fluorescence (living cells) of HepG2/Sor was stronger than that of HepG2 cells, indicating that the drug resistance of HepG2/Sor cells repressed the efficacy of Fe_3O_4@ZIF-8@Sor. Only a few living cells could be observed in both cells after the addition of Fe_3O_4@ZIF-8@Sor@TA, while after the addition of magnetic treatment, almost no living cells were observed in both cells, indicating that Fe_3O_4@ZIF-8@Sor@TA had the strongest therapeutic effect on HepG2 and HepG2-resistant cells when the composite was combined with magnetism.

3.6. Cellular Uptake Analysis. Cellular uptake of the drug was one of the indicators used to evaluate its bioavailability in the nanodrug delivery system. Since Fe_3O_4@ZIF-8@Sor@TA did not have fluorescent properties and could not be used to trace nanomaterials, we synthesized Fe_3O_4@ZIF-8@C-6@TA by using C-6 instead of Sor. Figure 5 presents the confocal laser scanning plots of HepG2/Sor cells co-incubated with free C-6, Fe_3O_4@ZIF-8@C-6, or Fe_3O_4@ZIF-8@C-6@TA for 4 h. Phalloidin could be used to stain the cytoplasm and DAPI could be used to stain the nucleus. Besides, C-6 could fluoresce green at 488 nm. Thus, HepG2/Sor cellular uptake of the material could be probed by fluorescence. The green fluorescence by C-6 was barely observed in cells in the free C-6 group and Fe_3O_4@ZIF-8@C-6, indicating that HepG2/Sor was ineffective for uptake. When HepG2/Sor was pretreated using TA and then co-incubated with Fe_3O_4@ZIF-8@C-6, intracellular C-6 fluorescence was significantly enhanced, indicating that TA intervention increased the uptake of the material by drug-resistant cells. Co-incubation of Fe_3O_4@ZIF-8@C-6@TA with HepG2/Sor revealed the most significant cellular uptake, indicating that delivery of Sor with Fe_3O_4@ZIF-8 as the drug carrier and modification of TA could effectively improve cellular uptake of Sor and hopefully increase the intra-tumor drug concentration and therapeutic effect.

3.7. Apoptosis Analysis. To investigate the induction of apoptosis of HepG2 and HepG2/Sor cells by Fe_3O_4@ZIF-8@Sor@TA composites, cell apoptosis with different materials was assayed using flow cytometry, and the results are presented in Figure 6. There was no significant apoptosis in the control group (PBS), and the apoptosis rate of HepG2 was slightly

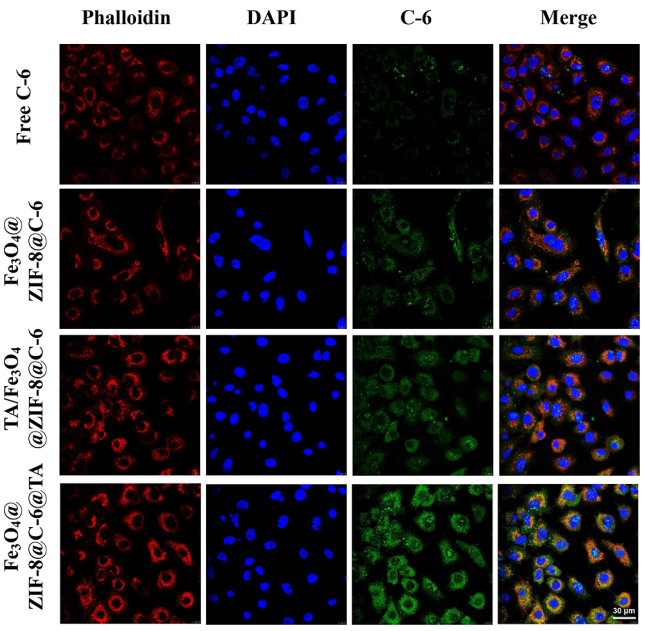

Figure 5. Confocal laser scanning plots of HepG2/Sor cells co-incubated with free C-6, Fe_3O_4@ZIF-8@C-6, and Fe_3O_4@ZIF-8@C-6@TA for 4 h (cytoskeleton and nucleus stained with phalloidin (red) and DAPI (blue), respectively).

higher than that of HepG2/Sor with free Sor treatment, indicating that the treatment became less effective when HepG2 cells were resistant to Sor. When Fe_3O_4@ZIF-8@Sor was added, the difference between the apoptosis rates of HepG2 and HepG2/Sor further increased, indicating that their therapeutic effect on drug-resistant cells was similarly low. The apoptosis rates of HepG2 and HepG2/Sor were further increased when the material continued to be modified with TA, which confirmed that TA modification could improve the therapeutic effect of the material on drug-resistant tumors. HepG2 and HepG2/Sor apoptosis rates were the highest when Fe_3O_4@ZIF-8@Sor@TA materials were magnetically induced, indicating that magnetic induction drove HepG2 and HepG2/Sor apoptosis.

3.8. In Vivo Antitumor Assessment and NIR Fluorescence Imaging Assay. To evaluate the antitumor activity of composite nanomaterials in vivo, we divided materials into PBS, free Sor, Fe_3O_4@ZIF-8@Sor@TA, and Fe_3O_4@ZIF-8@Sor@TA (magnetic), which were given to HepG2/Sor mice for 21 days. Figure 7a presents a change in mice's weight during different treatments. There was little change of weight when mice were given PBS, Fe_3O_4@ZIF-8@Sor@TA, and Fe_3O_4@ZIF-8@Sor@TA (magnetic) treatment, while there was a significant weight loss in mice given free Sor. The above phenomenon illustrated that the prepared Fe_3O_4@ZIF-8@Sor@TA nanomaterials were biocompatible and safe and could effectively avoid the side effects of Sor on mice. Tumor volumes of mice were calculated by measuring the long and short diameters of the tumors during treatment. The results, as shown in Figure 7b, presented that the tumors of mice in the PBS group grew at the fastest rate, indicating that the tumors had significant proliferative potential in the absence of drug intervention. The tumor volume of mice treated with the drug showed a decrease. The tumor volume of mice in the Fe_3O_4@ZIF-8@Sor@TA (magnetic) group decreased the most significantly compared to the free Sor, Fe_3O_4@ZIF-8@Sor@

https://doi.org/10.1021/acsomega.3c04215
ACS Omega 2023, 8, 39174−39185

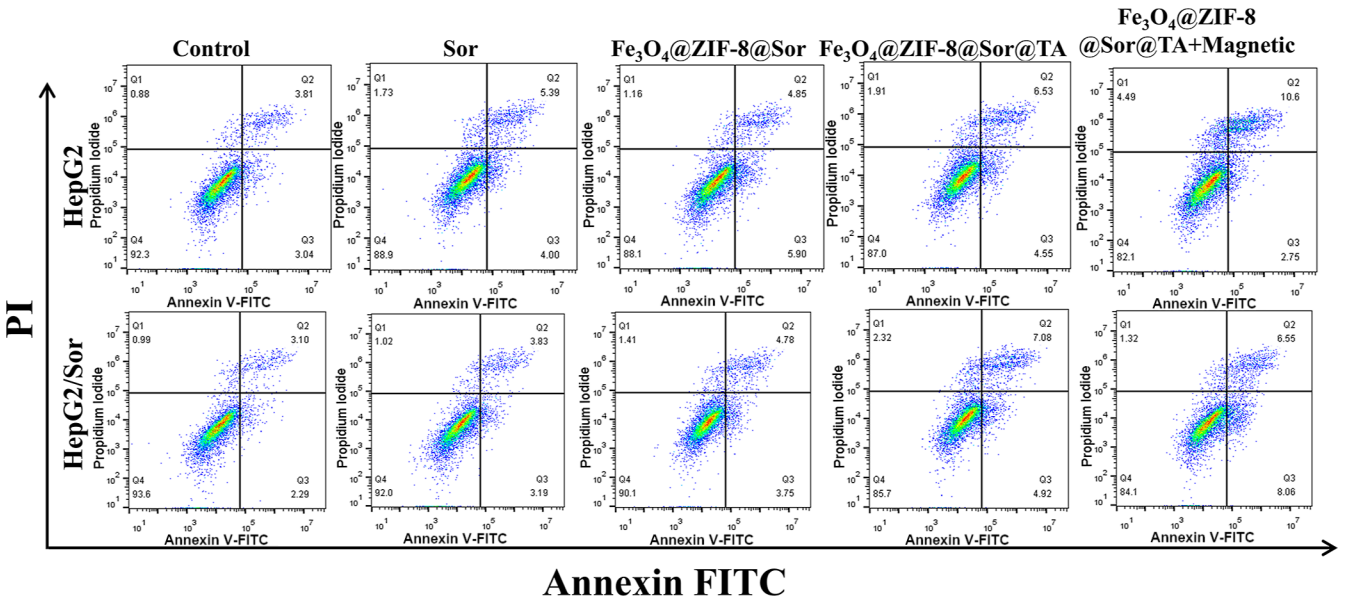

Figure 6. Apoptosis of HepG2 and HepG2/Sor cells with each group of materials.

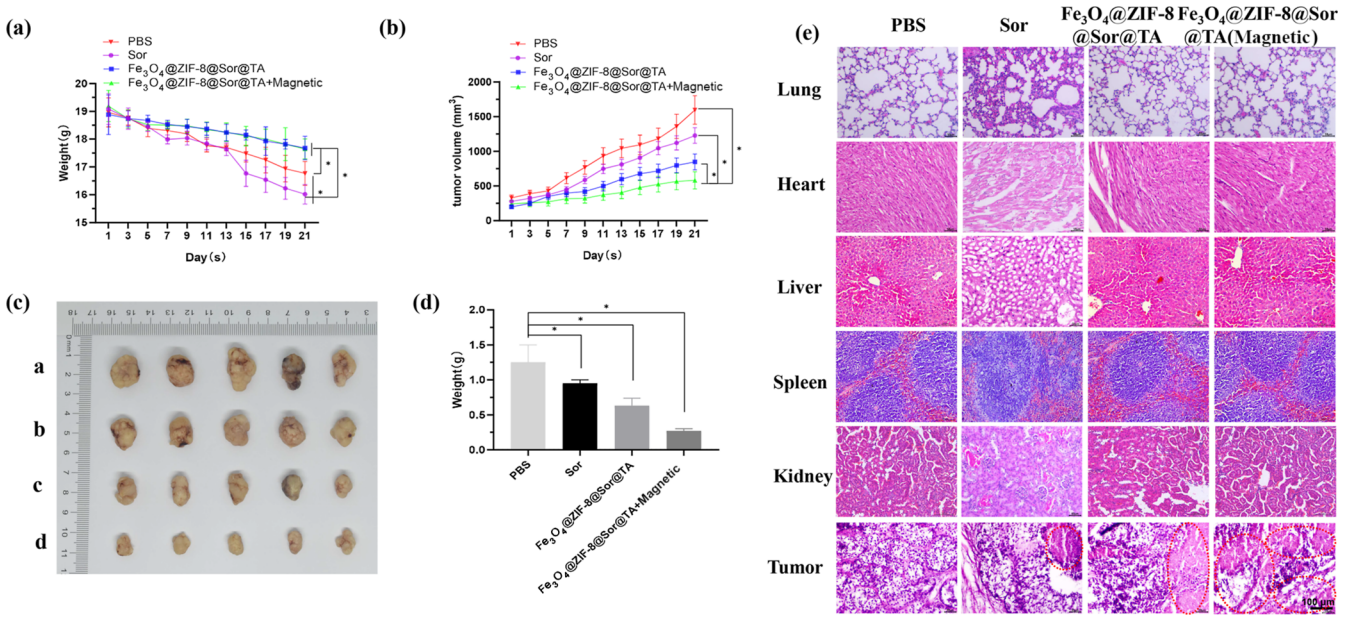

Figure 7. Evaluation of the effects of different drug treatments. (a) Plots of changes in weight of mice with different treatments; (b) plots of changes in tumor volume of mice with different treatments; (c) photographs of isolated tumors of mice with different treatments (a-PBS group; b-Sor; c-Fe_3O_4@ZIF-8@Sor@TA; and d-Fe_3O_4@ZIF-8@Sor@TA (magnetic)); (d) plots of changes in isolated tumor weights with different treatments (n = 5, *p < 0.05, **p < 0.01); and (e) H&E staining images of organs and tumor sections of mice treated with PBS, Sor, Fe_3O_4@ZIF-8@Sor@TA, and Fe_3O_4@ZIF-8@Sor@TA (magnetic).

TA, and Fe_3O_4@ZIF-8@Sor@TA (magnetic) groups, indicating the best cancer-repressive effect. This was a benefit of the magnetic targeting ability of Fe_3O_4@ZIF-8@Sor@TA. With a magnetic field, the material could actively target mouse tumor-bearing sites, prolong the circulation time of the drug in vivo, and respond to the tumor microenvironment, thus improving the bioavailability of Sor. To visualize the tumor size of mice in different treatment groups, mice were euthanized after 21 days of treatment, and tumors were excised and photographed (Figure 7c). The change in tumor size corresponded to the change in tumor volume, and all three groups showed tumor suppressive ability, among which Fe_3O_4@ZIF-8@Sor@TA (magnetic) had the strongest tumor suppressive potential. Figure 7d depicts plots of variation of tumor mass by weighing the isolated tumors. The average masses of tumors in groups of PBS, free Sor, Fe_3O_4@ZIF-8@Sor@TA, and Fe_3O_4@ZIF-8@Sor@TA (magnetic) were 1.25, 0.95, 0.63, and 0.27 g, respectively. These data illustrated the therapeutic potential of Fe_3O_4@ZIF-8@Sor@TA. After the mice were euthanized, the organs (heart, liver, spleen, lungs, and kidneys) and the tumor sites in the four groups were excised, fixed with 4% paraformaldehyde, embedded, sectioned, and stained with H&E for histopathological analysis. As presented in Figure 7e, organ sections of mice in the Sor group were damaged to varying degrees, implicating that free Sor treatment may cause unnecessary damage to the organs of mice. The morphological

https://doi.org/10.1021/acsomega.3c04215
ACS Omega 2023, 8, 39174−39185

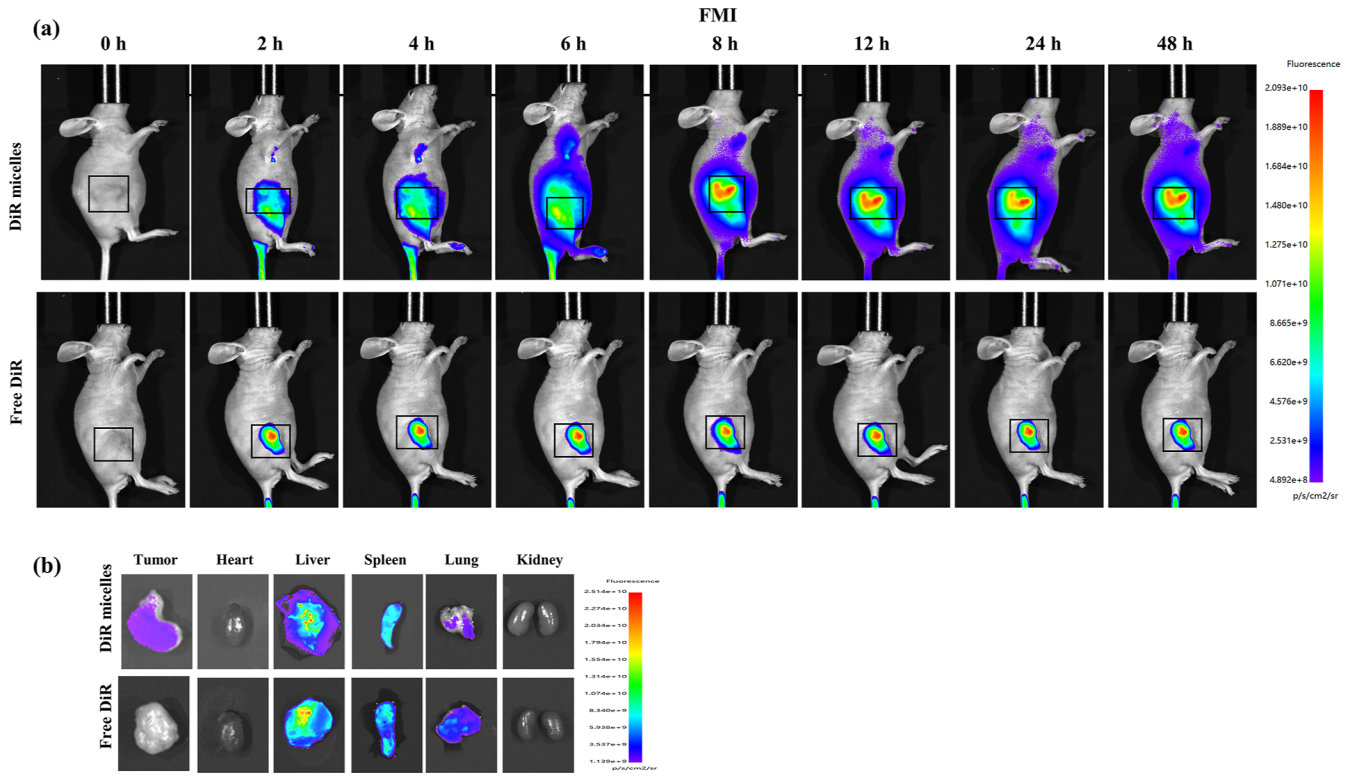

Figure 8. In vivo NIR fluorescence imaging. (a) In vivo fluorescence imaging within 48 h after injection with free DiR and Fe_3O_4@ZIF-8@DiR@TA (magnetic) and (b) ex vivo fluorescence imaging of tumors and organs after 48 h of injection with free DiR and Fe_3O_4@ZIF-8@DiR@TA (magnetic).

changes of the heart, liver, spleen, lung, and kidney sections of mice with the treatment of PBS, Fe_3O_4@ZIF-8@Sor@TA, and Fe_3O_4@ZIF-8@Sor@TA (magnetic) were not significantly damaged, indicating the superior biocompatibility and safety of the prepared Fe_3O_4@ZIF-8@Sor@TA, which could reduce the side effects on normal organs. Regarding tumor site sections, tumor cells in the PBS group showed a dense and regular distribution, while the other three groups presented different degrees of nuclei envelope wrinkling, indicating that the tumor tissue was damaged. By comparing the degree of damage with treatments of Sor, Fe_3O_4@ZIF-8@Sor@TA, and Fe_3O_4@ZIF-8@Sor@TA (magnetic), it could be seen that the lysis of cell nuclei was more significant in tumor sites of mice treated with Fe_3O_4@ZIF-8@Sor@TA (magnetic), which likewise confirmed the good antitumor activity of this composite.

To investigate the targeting and metabolic abilities of the injected Fe_3O_4@ZIF-8@Sor@TA in vivo, free DiR and Fe_3O_4@ZIF-8@DiR@TA with magnetical induction after tumor formation in mice and autoluminescence imaging was observed using BLI of the IVIS system at different times, respectively. As presented in Figure 8a, after the injection of Fe_3O_4@ZIF-8@DiR@TA for 2 h, the fluorescence signal of DiR was distributed throughout the mice. Still, the fluorescence of the tumor site was not much different from that of other sites. The fluorescence intensity of the tumor site increased gradually with the extension of the detection time, indicating the continuous accumulation of Fe_3O_4@ZIF-8@DiR@TA in the tumor site. At 12 h after injection, strong fluorescence was observed at the tumor site, while the fluorescence of the surrounding tissues gradually decreased. Finally, the strongest signal was seen in the tumor tissue at 48 h. In contrast, when the mice were injected with free DiR, a little fluorescent signal of DiR was observed at the tumor site regardless of the injection time. After 48 h of drug injection, mice were euthanized, and the tumors and organs were excised for ex vivo fluorescence imaging. As shown by the results of Figure 8b, the mice injected with Fe_3O_4@ZIF-8@DiR@TA (magnetic) had the strongest fluorescence signal intensity in the tumor tissue. In both groups of mice, the fluorescence intensity was stronger in the liver and spleen because the nanoparticles were metabolized mainly through the liver and spleen. In vivo NIR fluorescence imaging results illustrated that the synthesized nanoparticles were able to increase the accumulation and concentration of drugs at the tumor site, thus enhancing the therapeutic effect and bioavailability of drugs. Besides, Fe_3O_4@ZIF-8@Sor@TA was able to reduce the side effects on normal tissues and the damage to the organism.

4. DISCUSSION

HCC is a fatal malignancy that often exhibits poor treatment outcomes due to its advanced stage at the time of diagnosis.[42] At present, clinical treatment of HCC mainly includes surgery, chemotherapy, radiotherapy, targeted therapy, and immunotherapy.[43−45] Among them, post-surgical chemotherapy is the most predominant one for HCC, with a wide variety of chemotherapeutic agents such as cisplatin, 5-fluorouracil, Sor, and lenvatinib.[46−48] Despite chemotherapeutic drugs having therapeutic effects in a short period of time, prolonged administration produces drug resistance, leading to reduced therapeutic effects.[49] In other words, cytokine confusion and drug resistance generated after chemotherapy are the main factors that hinder the recovery of patients with advanced HCC. Therefore, exploring ways to counteract drug resistance

https://doi.org/10.1021/acsomega.3c04215
ACS Omega 2023, 8, 39174−39185

in clinical practice is an avenue to think about addressing chemotherapy failure. Nanomaterials have also been used in the pharmaceutical field in recent years due to their low toxicity, degradability, and high drug-loading capacity. Zhang et al.[50] synthesized a bifunctional liposome (Gal-P123-LPG) capable of targeting galactosyl and repressing P-glycoprotein (P-gp) and loaded with mitoxantrone. Their experimental results demonstrated that the composite is highly inhibitory against HCC in vivo and in vitro, can actively target tumor sites, and improves drug resistance by reducing P-gp. Zhang et al.[51] developed a hollow polydopamine composite nanodrug loaded with an inhibitor of the PI3K/mTOR signaling pathway (PKI-587) and the chemotherapeutic drug oxaliplatin, which has both a high drug-loading capacity and the ability to repair DNA damage and enhance apoptosis by regulating upstream and downstream genes. In this experiment, we designed a TA-coated Fe_3O_4@ZIF-8@Sor. In this system, many gallic acyl groups in the TA structure can interact with the regulatory region of P-gp and repress the function of P-gp by affecting ATPase activity,[52] which can effectively reverse drug resistance. Fe_3O_4@ZIF-8 is a nanoparticle with superparamagnetic properties and a large specific surface area that can be used to deliver drugs to the corresponding sites via magnetic targeting.[53]

In the scope of this study, we devised a multifunctional antitumor nanodrug by creating a complex involving Fe_3O_4@ZIF-8-Sor, which was further encapsulated with TA. Numerous analogous investigations have focused on developing nanomaterial-based drug carriers to augment controlled drug release capabilities.[54] Similarly, in our research, the ZIF-8-based architecture demonstrated the ability to enhance the rate of drug release within an acidic environment, aligning with the existing body of work aiming for improved drug delivery systems. Concurrently, the utilization of external stimuli, including magnetic fields, X-rays, ultrasound, and gas activation, to augment the potential of chemodynamic therapy has emerged as a prominent modality for enhancing the efficacy of nanomaterial-based pharmaceuticals.[55] Motivated by this evolving paradigm, we also employed magnetic augmentation to potentiate the therapeutic efficiency of our drug, thereby contributing to the advancement of this field. The experimental results presented that the synthesized Fe_3O_4@ZIF-8@Sor@TA nanospheres were around 150 nm in size and uniformly dispersed. The presence of Sor and TA was also demonstrated by FTIR, XRD, and UV characterization. Compared to the Fe_3O_4 encapsulation ratio prepared by the conventional method (15.2%),[56] the encapsulation ratio of our prepared Fe_3O_4@ZIF-8 on Sor was 40%, indicating that the complexation of ZIF-8 with Fe_3O_4 was able to improve the drug-loading rate. Continuing the in vitro cellular experiments on the materials, we found that our prepared Fe_3O_4@ZIF-8@Sor@TA was biocompatible with normal cells in general and suppressed two kinds of HCC cells with a higher affinity for HepG2. The material we prepared addresses the shortcomings of conventional Sor drugs in terms of their toxic effects on normal tissues. Lachaier et al.[57] manifested that Sor induces ferroptosis in patients to a large extent. When the material acted simultaneously with HepG2/Sor-resistant cells, it also showed superior antidrug resistance. This is promising to solve the challenge of tumor chemotherapy failure due to the development of drug resistance in tumors, as previously studied.[58] In vivo, antitumor experiments of the material revealed that its damage to other organs under magnetically induced conditions was minimal, probably due to the good magnetic targeting of Fe_3O_4@ZIF-8. Conventional nanomaterials are mostly modified with targeting aptamers,[59] targeting drugs,[60] or targeting carriers[61] when applied to tumor site targeting delivery, but such approaches are limited in cumbersome preparation methods and unstable materials. The material we generated could localize the tumor site using magnetic induction and was easy to prepare and well-targeted, making it an easy-to-use material with good therapeutic effects. H&E staining and in vivo NIR fluorescence imaging of mouse tumor tissues and organ sections illustrated its fewer toxic effects on normal tissues and stronger cumulative effects at tumor sites in living organisms. In summary, the Fe_3O_4@ZIF-8@Sor@TA nanocomposite drug had great advantages in targeting therapy, reducing Sor resistance, and improving the therapeutic effect on HCC, with promising clinical application.

5. CONCLUSIONS

We reported a multifunctional Fe_3O_4@ZIF-8@Sor@TA nanocomposite drug, which could solve the shortcomings of insufficient targeting and the generation of Sor resistance. The presence of Fe_3O_4 in Fe_3O_4@ZIF-8@Sor@TA enabled the material to actively target the tumor site under the induction of a magnetic field. The pH responsiveness of ZIF-8 helped the material rapidly release Sor to improve the therapeutic effect in the tumor microenvironment. Finally, TA could modulate the ability of ATPase to hinder P-gp function and reverse the development of drug resistance. Through in vivo and in vitro experiments, we could conclude that Fe_3O_4@ZIF-8@Sor@TA could effectively target tumor tissues and release Sor, reversing the Sor-resistant effect already developed by HepG2 cells and killing tumors. While our study extensively examined the efficacy of our nanodrug from various perspectives, certain limitations persist. Notably, we lack direct cellular or in-tissue observations of the magnetic effects on nanodrug efficacy. While numerous assays supported the positive impact of magnetic treatment through analyses of cell function and tumorigenesis in mouse models, we did not ascertain whether the magnetic treatment could effectively enhance the rate of drug uptake. Hence, this simple and low-cost composite nanodrug has a promising application in the field of cancer therapy and generates a novel insight into clinical treatment.

AUTHOR INFORMATION

Corresponding Authors

Yun Zhao − *Department of General Surgery, Xiangyang No. 1 People's Hospital, Hubei University of Medicine, Xiangyang City 441000, China*; Phone: +86-13972299040; Email: 53975980@qq.com

Peng Zhang − *Department of General Surgery, Xiangyang No. 1 People's Hospital, Hubei University of Medicine, Xiangyang City 441000, China*; orcid.org/0000-0002-2837-1677; Phone: +86-18307216591; Email: zhang1215peng@163.com

Authors

Jianqiao Kong − *Department of General Surgery, Xiangyang No. 1 People's Hospital, Hubei University of Medicine, Xiangyang City 441000, China*

Song Xu − *Department of General Surgery, Xiangyang No. 1 People's Hospital, Hubei University of Medicine, Xiangyang City 441000, China*

https://doi.org/10.1021/acsomega.3c04215
ACS Omega 2023, 8, 39174−39185

Yang Dai − *Department of General Surgery, Xiangyang No. 1 People's Hospital, Hubei University of Medicine, Xiangyang City 441000, China*

Yi Wang − *Department of General Surgery, Xiangyang No. 1 People's Hospital, Hubei University of Medicine, Xiangyang City 441000, China*

Complete contact information is available at: https://pubs.acs.org/10.1021/acsomega.3c04215

Author Contributions

Jianqiao Kong and Song Xu authors contributed equally. (I) Conception and design: Jianqiao Kong and Yun Zhao. (II) Administrative support: Yi Wang. (III) Provision of study materials or patients: Yi Wang. (IV) Collection and assembly of data: Peng Zhang. (V) Data analysis and interpretation: Jianqiao Kong. (VI) Manuscript writing: Jianqiao Kong, Yun Zhao, and Peng Zhang. (VII) Final approval of manuscript: All authors.

Funding

This study was supported by Innovative Research Program of Xiangyang No.1 People's Hospital (No.XYY2023QT16).

Notes

The authors declare no competing financial interest.

This study was approved by the Xiangyang No. 1 People's Hospital and the Hubei University of Medicine Animal Ethics Committee.

REFERENCES

(1) Anwanwan, D.; Singh, S. K.; Singh, S.; Saikam, V.; Singh, R. Challenges in liver cancer and possible treatment approaches. *Biochim. Biophys. Acta, Rev. Cancer* **2020**, *1873*, 188314.

(2) Orcutt, S. T.; Anaya, D. A. Liver Resection and Surgical Strategies for Management of Primary Liver Cancer. *Cancer Control* **2018**, *25*, 107327481774462.

(3) Zhou, H.; Song, T. Conversion therapy and maintenance therapy for primary hepatocellular carcinoma. *BioSci. Trends* **2021**, *15*, 155−160.

(4) Maki, H.; Hasegawa, K. Advances in the surgical treatment of liver cancer. *BioSci. Trends* **2022**, *16*, 178−188.

(5) Zhong, G.; Yang, C.; Liu, S.; Zheng, Y.; Lou, W.; Teo, J. Y.; Bao, C.; Cheng, W.; Tan, J. P.; Gao, S.; et al. Polymers with distinctive anticancer mechanism that kills MDR cancer cells and inhibits tumor metastasis. *Biomaterials* **2019**, *199*, 76−87.

(6) Lin, M.; Yao, W.; Xiao, Y.; Dong, Z.; Huang, W.; Zhang, F.; Zhou, X.; Liang, M. Resveratrol-modified mesoporous silica nanoparticle for tumor-targeted therapy of gastric cancer. *Bioengineered* **2021**, *12*, 6343−6353.

(7) Moradi, O.; Mahdavian, L. Simulation and computational study of graphene oxide nano-carriers, absorption, and release of the anticancer drug of camptothecin. *J. Mol. Model.* **2021**, *27*, 251.

(8) Munir, M. U.; Salman, S.; Javed, I.; Bukhari, S. N. A.; Ahmad, N.; Shad, N. A.; Aziz, F. Nano-hydroxyapatite as a delivery system: overview and advancements. *Artif. Cells, Nanomed., Biotechnol.* **2021**, *49*, 717−727.

(9) Namgung, R.; Mi Lee, Y.; Kim, J.; Jang, Y.; Lee, B. H.; Kim, I. S.; Sokkar, P.; Rhee, Y. M.; Hoffman, A. S.; Kim, W. J. Poly-cyclodextrin and poly-paclitaxel nano-assembly for anticancer therapy. *Nat. Commun.* **2014**, *5*, 3702.

(10) Ren, W.; Chen, S.; Liao, Y.; Li, S.; Ge, J.; Tao, F.; Huo, Q.; Zhang, Y.; Zhao, Z. Near-infrared fluorescent carbon dots encapsulated liposomes as multifunctional nano-carrier and tracer of the anticancer agent cinobufagin in vivo and in vitro. *Colloids Surf., B* **2019**, *174*, 384−392.

(11) Xu, S.; Zhong, Y.; Nie, C.; Pan, Y.; Adeli, M.; Haag, R. Co-Delivery of Doxorubicin and Chloroquine by Polyglycerol Functionalized MoS2 Nanosheets for Efficient Multidrug-Resistant Cancer Therapy. *Macromol. Biosci.* **2021**, *21*, No. e2100233.

(12) Wu, M. X.; Yang, Y. W. Metal-Organic Framework (MOF)-Based Drug/Cargo Delivery and Cancer Therapy. *Adv. Mater.* **2017**, *29*, 1606134.

(13) Tong, P. H.; Zhu, L.; Zang, Y.; Li, J.; He, X. P.; James, T. D. Metal-organic frameworks (MOFs) as host materials for the enhanced delivery of biomacromolecular therapeutics. *Chem. Commun.* **2021**, *57*, 12098−12110.

(14) Abdelhamid, H. N. Zeolitic Imidazolate Frameworks (ZIF-8) for Biomedical Applications: A Review. *Curr. Med. Chem.* **2021**, *28*, 7023−7075.

(15) Wang, Q.; Sun, Y.; Li, S.; Zhang, P.; Yao, Q. Synthesis and modification of ZIF-8 and its application in drug delivery and tumor therapy. *RSC Adv.* **2020**, *10*, 37600−37620.

(16) Yu, S.; Wang, S.; Xie, Z.; Yu, S.; Li, L.; Xiao, H.; Song, Y. Hyaluronic acid coating on the surface of curcumin-loaded ZIF-8 nanoparticles for improved breast cancer therapy: An in vitro and in vivo study. *Colloids Surf., B* **2021**, *203*, 111759.

(17) Ju, G.; Liu, B.; Ji, M.; Jin, R.; Xu, X.; Xiao, Y.; Li, J.; Xu, D.; Huang, Y.; Hou, J. Folic Acid-Modified miR-491-5p-Loaded ZIF-8 Nanoparticles Inhibit Castration-Resistant Prostate Cancer by Regulating the Expression of EPHX1. *Front. Bioeng. Biotechnol.* **2021**, *9*, 706536.

(18) Deng, Z.; Lin, J.; Bud'ko, S. L.; Webster, B.; Kalin, T. V.; Kalinichenko, V. V.; Shi, D. Dual Targeting with Cell Surface Electrical Charge and Folic Acid via Superparamagnetic Fe(3)O(4)@Cu(2-x)S for Photothermal Cancer Cell Killing. *Cancers* **2021**, *13*, 5275.

(19) Wang, R.; Degirmenci, V.; Xin, H.; Li, Y.; Wang, L.; Chen, J.; Hu, X.; Zhang, D. PEI-Coated Fe(3)O(4) Nanoparticles Enable Efficient Delivery of Therapeutic siRNA Targeting REST into Glioblastoma Cells. *Int. J. Mol. Sci.* **2018**, *19*, 2230.

(20) Wang, X.; Ma, Q.; Wen, C.; Gong, T.; Li, J.; Liang, W.; Li, M.; Wang, Y.; Guo, R. Folic acid and deoxycholic acid derivative modified Fe(3)O(4) nanoparticles for efficient pH-dependent drug release and multi-targeting against liver cancer cells. *RSC Adv.* **2021**, *11*, 39804−39812.

(21) Shi, Z.; Wang, Y.; Xiao, T.; Dong, S.; Lan, T. Preparation and Thermal Decomposition Kinetics of a New Type of a Magnetic Targeting Drug Carrier. *ACS Omega* **2021**, *6*, 3427−3433.

(22) Kiru, L.; Zlitni, A.; Tousley, A. M.; Dalton, G. N.; Wu, W.; Lafortune, F.; Liu, A.; Cunanan, K. M.; Nejadnik, H.; Sulchek, T.; et al. In vivo imaging of nanoparticle-labeled CAR T cells. *Proc. Natl. Acad. Sci. U.S.A.* **2022**, *119*, No. e2102363119.

(23) Lee, J.-H.; Kim, B.; Kim, Y.; Kim, S. K. Ultra-high rate of temperature increment from superparamagnetic nanoparticles for highly efficient hyperthermia. *Sci. Rep.* **2021**, *11*, 4969.

(24) Roach, P.; McGarvey, D. J.; Lees, M. R.; Hoskins, C. Remotely triggered scaffolds for controlled release of pharmaceuticals. *Int. J. Mol. Sci.* **2013**, *14*, 8585−8602.

(25) Li, Y.; Yin, G.; Pu, X.; Chen, X.; Liao, X.; Huang, Z. Novel Bi-Functional 14-mer Peptides with Both Ovarian Carcinoma Cells Targeting and Magnetic Fe(3)O(4)Nanoparticles Affinity. *Materials* **2019**, *12*, 755.

(26) Tang, W.; Chen, Z.; Zhang, W.; Cheng, Y.; Zhang, B.; Wu, F.; Wang, Q.; Wang, S.; Rong, D.; Reiter, F. P.; et al. The mechanisms of sorafenib resistance in hepatocellular carcinoma: theoretical basis and therapeutic aspects. *Signal Transduction Targeted Ther.* **2020**, *5*, 87.

(27) Gounder, M. M.; Mahoney, M. R.; Van Tine, B. A.; Ravi, V.; Attia, S.; Deshpande, H. A.; Gupta, A. A.; Milhem, M. M.; Conry, R. M.; Movva, S.; et al. Sorafenib for Advanced and Refractory Desmoid Tumors. *N. Engl. J. Med.* **2018**, *379*, 2417−2428.

(28) Nagesh, P. K. B.; Hatami, E.; Chowdhury, P.; Kashyap, V.; Khan, S.; Hafeez, B.; Chauhan, S.; Jaggi, M.; Yallapu, M. Tannic Acid Induces Endoplasmic Reticulum Stress-Mediated Apoptosis in Prostate Cancer. *Cancers* **2018**, *10*, 68.

(29) Chowdhury, P.; Nagesh, P. K.; Hatami, E.; Wagh, S.; Dan, N.; Tripathi, M. K.; Khan, S.; Hafeez, B. B.; Meibohm, B.; Chauhan, S. C.;

et al. Tannic acid-inspired paclitaxel nanoparticles for enhanced anticancer effects in breast cancer cells. *J. Colloid Interface Sci.* **2019**, *535*, 133−148.
(30) Orlowski, P.; Kowalczyk, A.; Tomaszewska, E.; Ranoszek-Soliwoda, K.; Węgrzyn, A.; Grzesiak, J.; Celichowski, G.; Grobelny, J.; Eriksson, K.; Krzyzowska, M. Antiviral Activity of Tannic Acid Modified Silver Nanoparticles: Potential to Activate Immune Response in Herpes Genitalis. *Viruses* **2018**, *10*, 524.
(31) Rahman, M. M.; Rahaman, M. S.; Islam, M. R.; Hossain, M. E.; Mannan Mithi, F.; Ahmed, M.; Saldías, M.; Akkol, E. K.; Sobarzo-Sánchez, E. Multifunctional Therapeutic Potential of Phytocomplexes and Natural Extracts for Antimicrobial Properties. *Antibiotics* **2021**, *10*, 1076.
(32) Chen, M. C.; Annseles Rajula, S.; Bharath Kumar, V.; Hsu, C. H.; Day, C. H.; Chen, R. J.; Wang, T. F.; Viswanadha, V. P.; Li, C. C.; Huang, C. Y. Tannic acid attenuate AKT phosphorylation to inhibit UMUC3 bladder cancer cell proliferation. *Mol. Cell. Biochem.* **2022**, *477*, 2863−2869.
(33) Naus, P. J.; Henson, R.; Bleeker, G.; Wehbe, H.; Meng, F.; Patel, T. Tannic acid synergizes the cytotoxicity of chemotherapeutic drugs in human cholangiocarcinoma by modulating drug efflux pathways. *J. Hepatol.* **2007**, *46*, 222−229.
(34) Sunoqrot, S.; Orainee, B.; Alqudah, D. A.; Daoud, F.; Alshaer, W. Curcumin-tannic acid-poloxamer nanoassemblies enhance curcumin's uptake and bioactivity against cancer cells in vitro. *Int. J. Pharm.* **2021**, *610*, 121255.
(35) Wu, Y.; Li, B.; Wang, X.; Yu, S.; Pang, H.; Liu, Y.; Liu, X.; Wang, X. Magnetic metal-organic frameworks (Fe3O4@ZIF-8) composites for U(VI) and Eu(III) elimination: simultaneously achieve favorable stability and functionality. *Chem. Eng. J.* **2019**, *378*, 122105.
(36) Chen, G.; Yu, B.; Lu, C.; Zhang, H.; Shen, Y.; Cong, H. Controlled synthesis of Fe3O4@ZIF-8 nanoparticles for drug delivery. *CrystEngComm* **2018**, *20*, 7486−7491.
(37) Zhang, T.; Zhang, X.; Yan, X.; Kong, L.; Zhang, G.; Liu, H.; Qiu, J.; Yeung, K. L. Synthesis of Fe3O4@ZIF-8 magnetic core−shell microspheres and their potential application in a capillary microreactor. *Chem. Eng. J.* **2013**, *228*, 398−404.
(38) Liu, L.; Ge, C.; Zhang, Y.; Ma, W.; Su, X.; Chen, L.; Li, S.; Wang, L.; Mu, X.; Xu, Y. Tannic acid-modified silver nanoparticles for enhancing anti-biofilm activities and modulating biofilm formation. *Biomater. Sci.* **2020**, *8*, 4852−4860.
(39) Aguilera, J. R.; Venegas, V.; Oliva, J. M.; Sayagués, M. J.; de Miguel, M.; Sánchez-Alcázar, J. A.; Arévalo-Rodríguez, M.; Zaderenko, A. P. Targeted multifunctional tannic acid nanoparticles. *RSC Adv.* **2016**, *6*, 7279−7287.
(40) Huo, J.-B.; Xu, L.; Yang, J. C. E.; Cui, H. J.; Yuan, B.; Fu, M. L. Magnetic responsive Fe3O4-ZIF-8 core-shell composites for efficient removal of As(III) from water. *Colloids Surf., A* **2018**, *539*, 59−68.
(41) Meng, X.; Jia, K.; Sun, K.; Zhang, L.; Wang, Z. Smart responsive nanoplatform via in situ forming disulfiram-copper ion chelation complex for cancer combination chemotherapy. *Chem. Eng. J.* **2021**, *415*, 128947.
(42) Demir, T.; Lee, S. S.; Kaseb, A. O. Systemic therapy of liver cancer. *Adv. Cancer Res.* **2021**, *149*, 257−294.
(43) Zhao, Y.; Zhang, Y. N.; Wang, K. T.; Chen, L. Lenvatinib for hepatocellular carcinoma: From preclinical mechanisms to anti-cancer therapy. *Biochim. Biophys. Acta, Rev. Cancer* **2020**, *1874*, 188391.
(44) Munoz-Martinez, S.; Iserte, G.; Sanduzzi-Zamparelli, M.; Llarch, N.; Reig, M. Current pharmacological treatment of hepatocellular carcinoma. *Curr. Opin. Pharmacol.* **2021**, *60*, 141−148.
(45) Uson Junior, P. L. S.; Nagalo, B. M.; Ahn, D. H.; Bekaii-Saab, T.; Borad, M. J. Combination Immunotherapy for Hepatocellular Carcinoma: Where Are We Currently? *Semin. Liver Dis.* **2021**, *41*, 136−141.
(46) Qin, S.; Bi, F.; Gu, S.; Bai, Y.; Chen, Z.; Wang, Z.; Ying, J.; Lu, Y.; Meng, Z.; Pan, H.; et al. Donafenib Versus Sorafenib in First-Line Treatment of Unresectable or Metastatic Hepatocellular Carcinoma: A Randomized, Open-Label, Parallel-Controlled Phase II-III Trial. *J. Clin. Oncol.* **2021**, *39*, 3002−3011.
(47) Wang, F.; Xu, C.; Li, G.; Lv, P.; Gu, J. Incomplete radiofrequency ablation induced chemoresistance by up-regulating heat shock protein 70 in hepatocellular carcinoma. *Exp. Cell Res.* **2021**, *409*, 112910.
(48) Torrens, L.; Montironi, C.; Puigvehí, M.; Mesropian, A.; Leslie, J.; Haber, P. K.; Maeda, M.; Balaseviciute, U.; Willoughby, C. E.; Abril-Fornaguera, J.; et al. Immunomodulatory Effects of Lenvatinib Plus Anti-Programmed Cell Death Protein 1 in Mice and Rationale for Patient Enrichment in Hepatocellular Carcinoma. *Hepatology* **2021**, *74*, 2652−2669.
(49) Wang, C. I.; Chu, P. M.; Chen, Y. L.; Lin, Y. H.; Chen, C. Y. Chemotherapeutic Drug-Regulated Cytokines Might Influence Therapeutic Efficacy in HCC. *Int. J. Mol. Sci.* **2021**, *22*, 13627.
(50) Zhang, X.; Guo, S.; Fan, R.; Yu, M.; Li, F.; Zhu, C.; Gan, Y. Dual-functional liposome for tumor targeting and overcoming multidrug resistance in hepatocellular carcinoma cells. *Biomaterials* **2012**, *33*, 7103−7114.
(51) Zhang, Y. C.; Wu, C. G.; Li, A. M.; Liang, Y.; Ma, D.; Tang, X. L. Oxaliplatin and Gedatolisib (PKI-587) Co-Loaded Hollow Polydopamine Nano-Shells with Simultaneous Upstream and Downstream Action to Re-Sensitize Drugs-Resistant Hepatocellular Carcinoma to Chemotherapy. *J. Biomed. Nanotechnol.* **2021**, *17*, 18−36.
(52) Li, H.; Krstin, S.; Wink, M. Modulation of multidrug resistant in cancer cells by EGCG, tannic acid and curcumin. *Phytomedicine* **2018**, *50*, 213−222.
(53) Zhang, Y.; Yang, Y.; Shi, J.; Wang, L. A multimodal strategy of Fe(3)O(4)@ZIF-8/GOx@MnO(2) hybrid nanozyme via TME modulation for tumor therapy. *Nanoscale* **2021**, *13*, 16571−16588.
(54) Xue, X.; Qu, H.; Li, Y. Stimuli-responsive crosslinked nanomedicine for cancer treatment. *Exploration* **2022**, *2*, 20210134.
(55) Jana, D.; Zhao, Y. Strategies for enhancing cancer chemodynamic therapy performance. *Exploration* **2022**, *2*, 20210238.
(56) Gong, T.; Dong, Z.; Fu, Y.; Gong, T.; Deng, L.; Zhang, Z. Hyaluronic acid modified doxorubicin loaded Fe(3)O(4) nanoparticles effectively inhibit breast cancer metastasis. *J. Mater. Chem. B* **2019**, *7*, 5861−5872.
(57) Lachaier, E.; et al. Sorafenib induces ferroptosis in human cancer cell lines originating from different solid tumors. *Anticancer Res.* **2014**, *34*, 6417−6422.
(58) Cheng, Z.; Wei-Qi, J.; Jin, D. New insights on sorafenib resistance in liver cancer with correlation of individualized therapy. *Biochim. Biophys. Acta, Rev. Cancer* **2020**, *1874*, 188382.
(59) He, F.; Wen, N.; Xiao, D.; Yan, J.; Xiong, H.; Cai, S.; Liu, Z.; Liu, Y. Aptamer-Based Targeted Drug Delivery Systems: Current Potential and Challenges. *Curr. Med. Chem.* **2020**, *27*, 2189−2219.
(60) Elgohary, M. M.; Helmy, M. W.; Mortada, S. M.; Elzoghby, A. O. Dual-targeted nano-in-nano albumin carriers enhance the efficacy of combined chemo/herbal therapy of lung cancer. *Nanomedicine* **2018**, *13*, 2221−2224.
(61) Gao, M.; Deng, H.; Zhang, W. Hyaluronan-based Multifunctional Nano-carriers for Combination Cancer Therapy. *Curr. Top. Med. Chem.* **2021**, *21*, 126−139.

https://doi.org/10.1021/acsomega.3c04215
ACS Omega 2023, 8, 39174−39185